JOM, Vol. 73, No. 12, 2021
https://doi.org/10.1007/s11837-021-04908-3

Effect of Mn on Microstructure and Mechanical Properties of Al-4Ni Alloy

JIAO FANG,[1] XIXI DONG,[1] and SHOUXUN JI [1,2]

1.—Brunel Centre for Advanced Solidification Technology (BCAST), Brunel University London, Uxbridge UB8 3PH, Middlesex, UK. 2.—e-mail: shouxun.ji@brunel.ac.uk

The application of aluminum alloys at elevated temperatures has been attractive for decades, and Al-Ni-based alloys have recently been recognized as potential candidates. The effect of Mn on Al-4Ni alloy has been investigated in this work. Addition of Mn transformed the eutectics from Al_3Ni/α-Al to $Al_9(Ni,Mn)_2$/α-Al phases. Mn also improved the tensile strength at both 25°C and 250°C. The yield strength at 25°C increased from 48 MPa to 92 MPa with 1.87% Mn and then to 117 MPa with 3.77% Mn. At 250°C, the yield strength increased from 35 MPa to 82 MPa with 1.87% Mn and then to 101 MPa with 3.77% Mn. The alloys with Mn also showed less strength loss than Al-4Ni alloy at 250°C. The eutectic $Al_9(Ni,Mn)_2$ phase showed good thermal stability. No coarsening was observed after 2000 h at 250°C.

INTRODUCTION

The development of aluminum alloys for application at elevated temperatures has been attractive and an important topic for several decades. Cast Al-Si-based alloys are very commonly used in engine manufacturing. However, Al-Si-based alloys with Si content varying from 6% to 12% are typically limited to use below 175°C.[1] Above this temperature, their mechanical properties degrade rapidly as a result of dispersoid and precipitate coarsening[2,3] In addition, the development of diesel and direct fuel injection gasoline engines with high specific powers has posed challenges to existing Al-Si alloys due to the requirement for increased working pressures and temperatures that call for aluminum alloys capable of working at higher temperatures.

Considerable efforts have been made from different aspects to improve the mechanical performance of aluminum alloys at elevated temperatures. One attempt aimed to modify Al-Si alloys with heat-resistant Al_3X dispersoids and precipitates. Transition metals such as Sc, Zr, Ti, V, and Ni[4–13] were found to be effective. However, the volume fraction of Al_3X phase obtained through precipitation is usually very low, and some of these elements are very expensive, thus limiting industrial applications of such materials. Other attempts aimed to develop new alloys such as Al-Fe-V-Si, Al-Fe-Mo-V, Al-Fe-Gd, and Al-Ni-Y-Co.[14–17] Some of these alloys require rapid solidification to improve their effectiveness, and it is difficult to achieve satisfactory results using conventional casting methods. Therefore, their high cost and technological difficulties in producing large-size and complex-shaped parts are unavoidable hurdles for industrial applications.

Attempts to use the Al–Ni–Mn system have been made over the past few years.[18–20] The main reasons are that the Al–Ni binary system has a higher eutectic temperature (~ 640°C) and the Al_3Ni phase is stable up to 600°C,[21,22] offering potential for application at elevated temperatures. The microstructures of Al-Ni-Mn alloys obtained at a cooling rate of 90 K/s and 5 K/s have been investigated.[20] The eutectic structure was reported to be α-Al/Al_3Ni, and an O phase was observed. However, many open questions regarding the Al–Ni–Mn system remain, in particular the effect of Mn on the microstructure and mechanical properties at room and elevated temperatures and the thermal stability of Al-Ni-Mn alloys.

Therefore, in the work presented herein, we aimed to study the effect of Mn on the microstructure and mechanical properties of Al-4Ni (all compositions hereafter in wt.% unless otherwise specified) alloy processed by permanent mold

(Received June 10, 2021; accepted September 13, 2021; published online October 15, 2021)

casting. Because the eutectic point of binary Al-Ni alloy contains 5.69% Ni, the hypoeutectic Al-4Ni alloy was expected to be able to provide good castability and sufficient eutectic phases to balance the manufacturing and mechanical properties. Three levels of Mn were introduced to investigate the formation of Mn-containing intermetallic phase and the effect on the mechanical performance. The microstructure and mechanical properties were examined at both 25°C and 250°C. The discussion focuses on the microstructure, strengthening mechanism, and thermal stability of the Al-Ni-Mn alloys.

EXPERIMENTAL PROCEDURES

Alloy Preparation and Casting

Four experimental alloys (Al-4Ni, Al-4Ni-2Mn, Al-4Ni-3Mn, and Al-4Ni-4Mn) were prepared by melting Al-20Ni and Al-20Mn master alloys with pure aluminum (99.8%) in an electric resistance furnace at 800°C. The melt was held for at least 1 h before degassing with Ar using a rotary degasser at 300 rpm for 5 min. The melt temperature was then recovered to 750°C, followed by casting into a steel mold designed according to ASTM B-108, resulting in two standard tensile bars with gauge length of 50 mm and diameter of 10 mm. The compositions of the experimental alloys were determined by inductively coupled plasma optical emission spectrometry (ICP-OES). The actual and nominal compositions are Al-4.04Ni (used as Al-4Ni), Al-4.24Ni-1.87Mn (used as Al-4Ni-2Mn), Al-4.0Ni-3.01Mn (used as Al-4Ni-3Mn), and Al-3.82Ni-3.77Mn (used as Al-4Ni-4Mn). Impurities were well controlled. The contents of Fe and Si were under 0.18 and 0.10, respectively.

Microstructure Analysis and Tensile Testing

Samples for scanning electron microscopy (SEM) investigation were taken from the middle of tensile testing bars and prepared using standard metallographic techniques. To reveal the morphology of phases, deep etching was performed with 10 vol.% HCl solution for 10 min to 20 min. Microstructures were characterized using a ZEISS SUPRA™ 35VP SEM. Quantitative analysis was performed using a JEOL JXA−8230 electron probe microanalyzer (EPMA) coupled with wavelength-dispersive spectroscopy (WDS) detectors, operating at 15 kV. Samples for transmission electron microscopy (TEM) were prepared by using a Gatan Precision ion polishing system (PIPs). Foils were characterized by JEOL JEM-2100F at a working voltage of 200 kV.

Tensile testing was conducted using an Instron 5569 electromechanical system. For the test at ambient temperature (25°C), the extension rate was set at 1 mm/min using an extensometer with 50 mm gauge length (Instron Static Axial Clip-on Extensometer, 2630-113). For testing at 250°C, the samples were placed in a ventilated environmental chamber that can be controlled at ± 2°C. During testing, the samples were preheated to 250°C and maintained at this temperature for 40 min in the chamber before applying tension. Since the extensometer could not work at 250°C, the elongation was obtained from accurately positioned lines on the gauge length of 50 mm and measured using a micrometer before and after the tensile test. A minimum of three measurements were taken for each sample, and the average was taken as the result. Hardness testing was conducted using a 432 SVD digital auto turret macro–Vickers hardness tester using a load of 10 kg and dwell time of 10 s. A minimum of eight measurements were taken for each sample, and the average was taken as the result.

RESULTS AND DISCUSSION

Microstructure

The typical microstructures of the Al-4Ni and Al-4Ni-2Mn alloys are shown in Fig. 1. These two alloys displayed similar microstructure comprising primary α-Al dendrites and eutectic phases. In the Al-4Ni alloy, the primary α-Al contained 0.28% Ni, while in the Al-4Ni-2Mn alloy, the α-Al contained about 0.43% Ni and 1.6% Mn. Ni shows very limited solubility in Al,[21] while Mn has a maximum solubility of 1.8% in Al.[23] Hence, the concentration of Mn in α-Al is much higher than that of Ni. The eutectic intermetallic phase in both the Al-4Ni and Al-4Ni-2Mn alloys showed rod-like shape. The eutectic intermetallic phase in the Al-4Ni alloy showed a composition of Al-23.4 at.%Ni, which is a typical Al_3Ni phase according to the equilibrium phase diagram of Al–Ni binary alloys.[21] The eutectic intermetallic phase in the Al-4Ni-2Mn alloy, however, showed the composition Al-13.5 at.%Ni -3.7 at.%Mn. Clearly, this is not Al_3Ni but closer to the $Al_9(Ni,Mn)_2$ phase, which is reported to have the monoclinic lattice structure of Al_9Co_2 phase with lattice parameters of a = 0.8585 nm, b = 0.6269 nm, c = 0.6205 nm, and β = 95.34°.[24] TEM micrographs and diffraction patterns of the intermetallic phase are presented in Fig. 1c, d, and e. The electron diffraction patterns were indexed to $Al_9(Ni,Mn)_2$ phase along zone axis [001] and [101]. Therefore, the eutectic intermetallic phase in the Al-4Ni-2Mn alloy was confirmed to be $Al_9(Ni,Mn)_2$ phase. Addition of Mn to Al-4Ni alloy resulted in a transformation of the eutectic structure from Al_3Ni/α-Al to $Al_9(Ni,Mn)_2$/α-Al. This is different from the eutectic intermetallic phase identified by previous studies,[18,22] in which the eutectic Al_3Ni phase was reported in Al-Ni-Mn alloys. $Al_9(Ni,Mn)_2$ phase was also observed in the works of Balanetskyy[24] and Yu.[25] $Al_9(Ni,Mn)_2$ phase has a Al_9Co_2-type lattice structure, which is similar to $Al_9(Fe,Ni)_2$ (also known as Al_9FeNi phase).[26] For the $Al_9(Fe,Ni)_2$ phase, both Ni and Fe possibly appear at sites that originally corresponded to Co in Al_9Co_2 phase.

This is most likely also the case for the $Al_9(Ni, Mn)_2$ phase. Both Ni and Mn can occupy each Co site, , thus the concentration of Ni and Mn may not be fixed. Balanetskyy[24] reported a composition of Al-14.7 at.%Ni-2.8 at.%Mn, while Yu[25] reported a composition of Al-16.5 at.%Ni-3.2 at.%Mn for the $Al_9(Ni,Mn)_2$ phase. In this paper, the composition for $Al_9(Ni,Mn)_2$ phase was measured as Al-13.5 at.%Ni -3.7 at.%Mn. Although the concentration of Ni and Mn may vary, the total amount of Ni and Mn remains at a level of 18 at.%. It is thus clear that addition of Mn to Al-4Ni alloy resulted in a transformation of the eutectic structure from Al_3Ni/α-Al to $Al_9(Ni,Mn)_2/\alpha$-Al.

Figure 2 shows the difference between the intermetallic phases in the Al-4Ni alloys with different Mn contents. In the Al-4Ni-3Mn alloy, two different primary intermetallic phases were observed. One was coarse gray particles showing hexagonal shapes with black cores inside (Fig. 2a). The core inside showed a composition of Al-1.35Mn-0.37Ni, which is α-Al. EPMA revealed the average composition of the hexagonal phase to be Al-15.6 at.%Mn-4.8 at.%Ni, corresponding to the formula $Al_{16.6}Mn_3Ni_1$. This hexagonal phase was identified as k-phase, which has a composition of Al-(14.7–18.9) at.%Mn-(1.3–5.9) at.%Ni.[24] The k-phase was reported to have the hexagonal lattice structure of $Al_{14.1}Cr_{3.4}Ni_{1.1}$ phase existing in Al-Cr-Ni and Al-Ni-Mn alloys.[27] Another, acicular morphology is shown in Fig. 2b for the intermetallic phase. The composition was measured to be Al-12.6 at.%Mn-7.0 at.%Ni, which is close to the formula $Al_{60}Mn_{11}Ni_4$. There are two lattice structures for the formula $Al_{60}Mn_{11}Ni_4$, viz. $Al_{60}Mn_{11}Ni_4$ and $C_{3,I}$-$Al_{60}Mn_{11}Ni_4$. $Al_{60}Mn_{11}Ni_4$ phase has orthorhombic structure with lattice parameters of a = 0.755 nm, b = 1.250 nm, and c = 2.380 nm, while $C_{3,I}$-$Al_{60}Mn_{11}Ni_4$ also has orthorhombic structure but with lattice parameters of a = 3.27 nm, b = 1.25 nm, and c = 2.38 nm. Obviously, both $C_{3,I}$-$Al_{60}Mn_{11}Ni_4$ and $Al_{60}Mn_{11}Ni_4$ are orthorhombic structures and the only difference lies in the value of the lattice parameter a. Hence, it is not easy to distinguish $C_{3,I}$-$Al_{60}Mn_{11}Ni_4$ from $Al_{60}Mn_{11}Ni_4$ without detailed TEM diffraction patterns. $Al_{60}Mn_{11}Ni_4$ was referred to as X-phase or R-phase in Refs. 28 and 29 but as O-phase in Ref. 20 Even earlier, Balanetskyy[24] referred to the $C_{3,I}$-$Al_{60}Mn_{11}Ni_4$ as O-phase, not $Al_{60}Mn_{11}Ni_4$. Because of this remaining uncertainty and as these two

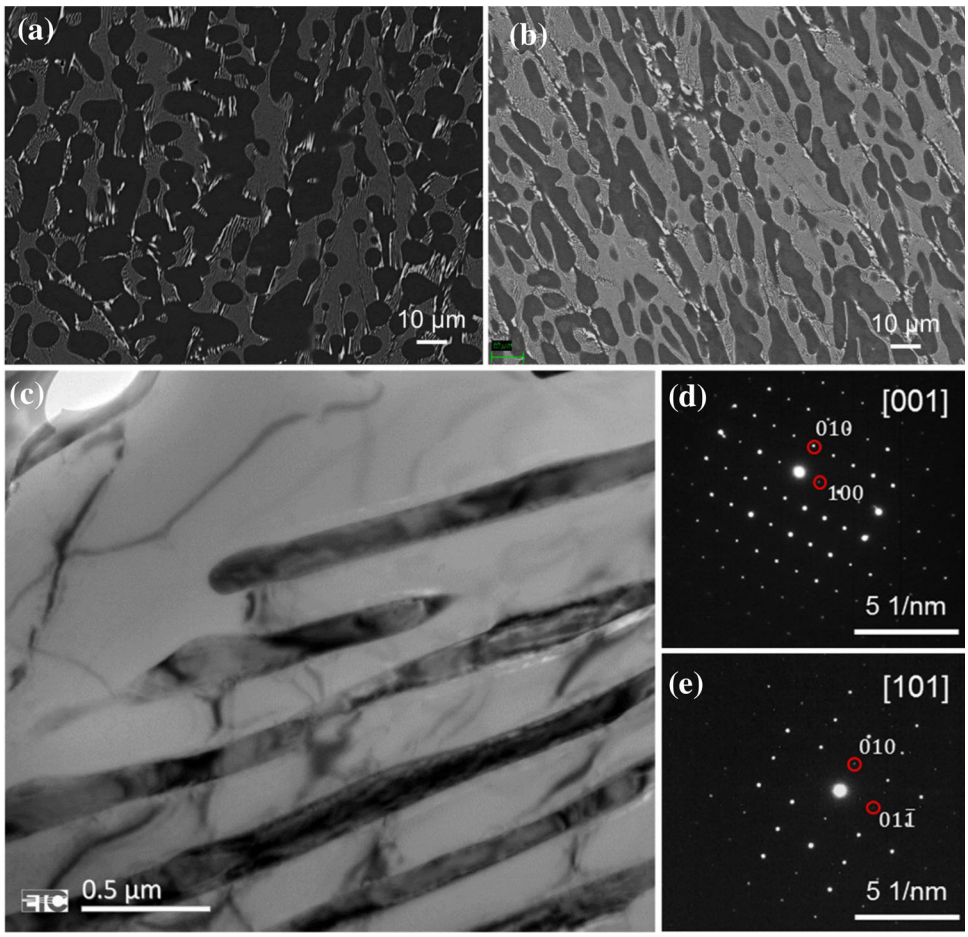

Fig. 1. SEM micrographs showing typical microstructure of (a) Al-4Ni alloy and (b) Al-4Ni-2Mn alloy. (c) TEM micrograph showing eutectic $Al_9(Ni,Mn)_2$ phase. Electron diffraction patterns along (d) [001] and (e) [101] zone axis.

phases are difficult to distinguish, we use O-phase for $Al_{60}Mn_{11}Ni_4$ phase in the present study.

The typical microstructures of Al-4Ni-4Mn alloy are presented in Fig. 2c, d. With increasing Mn level, the amount of intermetallic phase increased. Dendritic intermetallic is observed in Fig. 2c, and EDS analysis confirmed that it was k-phase. The size of k-phase increased, and the morphology also changed, when the Mn content in the Al-Ni alloys was increased. It changed from hexagonal shape with α-Al core inside to become massive dendritic shapes. Moreover, coarse Al_6Mn phase was also observed at a level of several hundred micrometers in the Al-4Ni-4Mn alloy, which displayed a well-developed dendritic morphology. With addition of 1.87% Mn, the eutectic structure transformed from α-Al/Al_3Ni to α-Al/$Al_9(Ni,Mn)_2$. When the Mn level was increased to 3.01, k-phase and O-phase were formed, and when the Mn level was increased further to 3.77%, Al_6Mn dendrites were observed.

Mechanical Performance at 25°C and 250°C

The hardness of the Al-Ni-Mn alloys with different Mn levels is shown in Fig. 3a. Clearly, the hardness increased linearly with increasing Mn level. The Al-4Ni alloy presented hardness of 42.3 HV_{10} while the Al-4Ni-2Mn alloy showed a 53% increase to 64.5 HV_{10}. When the Mn level was further increased to 3.01% and 3.77%, the hardness increased to 67.2 HV_{10} and 69.9 HV_{10}, respectively.

Figure 3b presents the tensile strength of the Al-4Ni-Mn alloys at ambient temperature (25°C). It is seen that the yield strength exhibited a significant increase with increasing Mn content. The yield strength was 48 MPa for the Al-4Ni alloy but 92 MPa for the Al-4Ni-2Mn alloy. When the Mn content was increased to 3.01% and 3.77%, the yield strength increased monotonically to 110 MPa and 117 MPa, respectively.

Strengthening of alloys can basically be classified into five mechanisms: solid-solution strengthening, second-phase strengthening, grain-boundary strengthening, precipitate strengthening, and strain hardening. The maximum solubility of Ni in α-Al is 0.05% at 640°C, which is negligible for solid-solution strengthening, while Mn has a maximum solubility of 1.8% in α-Al at 658°C.[23] The α-Al phase in experimental Al-4Ni-2Mn alloy contained 1.6% Mn. As the atomic radius of Mn is 1.40 Å while that of Al is 1.25 Å, the solid solution with Mn in Al results in lattice distortion, which hinders dislocation motion under loading. Therefore, addition of Mn introduces solid-solution strengthening in Al-Ni-Mn alloys.

On the other hand, increasing the level of Mn addition increased the amount of eutectic phases and primary intermetallic phases. The measured volume fractions of different phases in the experimental Al-4Ni-Mn alloys are presented in Table I. As seen, the Al-4Ni alloy contained 44 vol.% of eutectic phases. With 1.87% Mn addition, the eutectic phases increased to 51 vol.%, while no primary intermetallic phase was found. With 3.01% Mn addition, the eutectic phases increased to 58 vol.%, and the primary intermetallic phase was

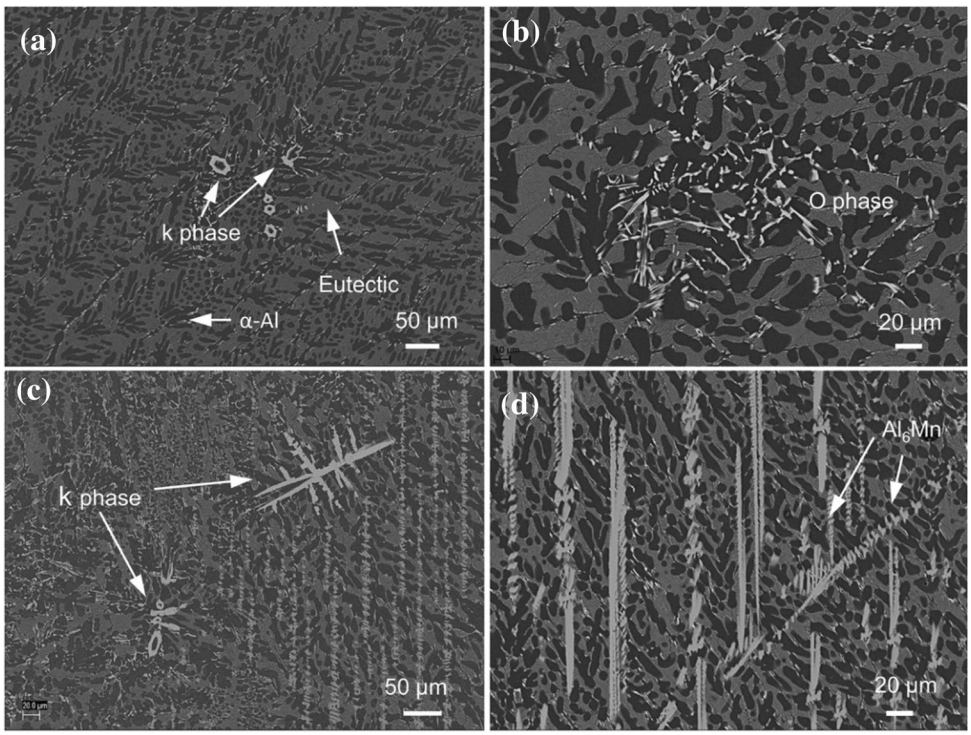

Fig. 2. Typical microstructure of intermetallic in (a, b) Al-4Ni-3Mn alloy and (c, d) Al-4Ni-4Mn alloy.

found at a level of 1 vol.%. When the Mn content was increased to 3.77%, the eutectic phases increased to 60 vol.% and the primary intermetallic phase increased to 5 vol.%. This increase in the eutectic phases and primary intermetallic phases can introduce second-phase strengthening. This can therefore explain the observed improvement in the yield strength on Mn addition.

The ultimate tensile strength also displayed significant improvement with increasing Mn content at ambient temperature. It increased dramatically from 129 MPa for the Al-4Ni alloy to 204 MPa for the Al-4Ni-2Mn alloy, then reached a peak strength of 227 MPa for 3.01% Mn. However, when the Mn content was increased further to 3.77%, the ultimate tensile strength did not increase but rather decreased slightly to 225 MPa. As presented in Fig. 2d, the dendritic Al_6Mn phase appeared in the Al-4Ni-4Mn alloy, having a size of several hundred micrometers. For this type of tough and large-size intermetallic phase, the localized stress on the particle surface and especially in the dendrite corners and tips increases quickly and accelerates fracture of the material. Therefore, the Al-4Ni-4Mn alloy presented lower ultimate tensile strength than the Al-4Ni-3Mn alloy. The elongation decreased dramatically with increasing Mn content, from 18.0% for the Al-4Ni alloy to 8.6% and 5.2% for the Al-4Ni-2Mn and Al-4Ni-3Mn alloys, respectively. For the Al-4Ni-4Mn alloy, the elongation was only 2.3%, indicating brittle fracture. This corroborates the decreased ultimate tensile strength of the Al-4Ni-4Mn alloy.

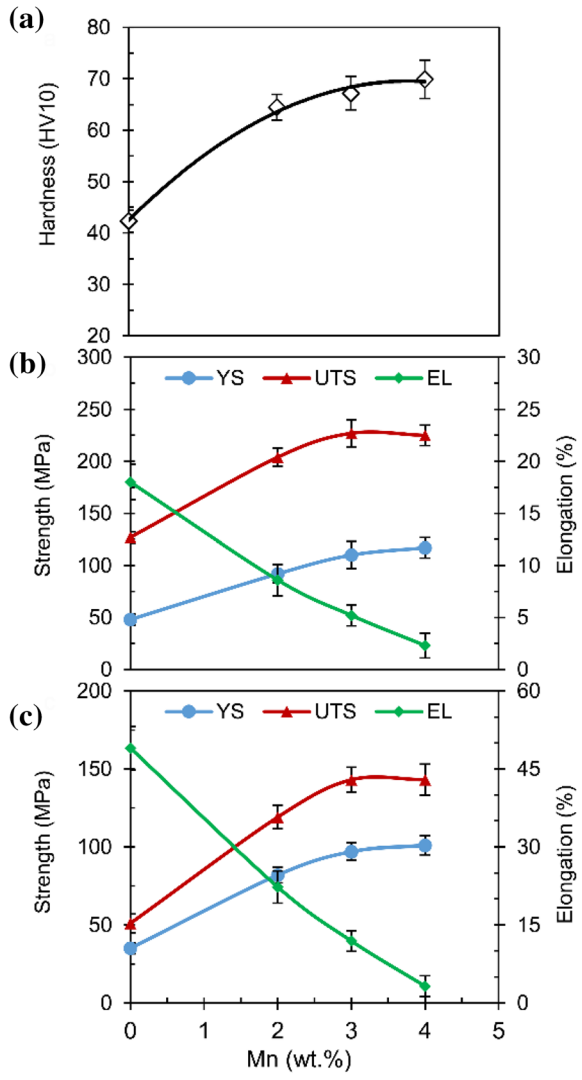

Fig. 3. (a) Effect of Mn content on hardness, and tensile property at (b) 25°C and (c) 250°C.

The tensile properties at 250°C are shown in Fig. 3c, revealing that Mn addition improved both the yield strength and ultimate tensile strength at this temperature. The yield strength was 35 MPa for the Al-4Ni alloy but 82 MPa for the Al-4Ni-2Mn alloy, corresponding to an increase of 134%. When the Mn level was increased to 3.01% and 3.77%, the yield strength increased monotonically to 96 MPa and 101 MPa, respectively. Meanwhile, the ultimate tensile strength increased from 51 MPa for the Al-4Ni alloy to 120 MPa for the Al-4Ni-2Mn alloy, then to 143 MPa when the Mn level was increased further to 3.77%. The elongation at 250°C was much higher than that at ambient temperature, but addition of Mn decreased the elongation dramatically at 250°C. The elongation was 49.0% for the Al-4Ni alloy and 17.9% for the Al-4Ni-2Mn alloy, but decreased further to 11.9% and 3.7% for the Al-4Ni-3Mn alloy and Al-4Ni-4Mn alloy, respectively.

Moreover, the alloys with Mn addition presented less strength loss when the temperature was increased to 250°C. Table II presents the strength loss of the experimental alloys. Clearly, the alloys with Mn addition presented less strength loss. The Al-4Ni alloy showed a reduction of 27% in the yield strength between 25°C and 250°C. However, the Al-4Ni-2Mn alloy showed only 10% yield strength loss. Meanwhile, the Al-4Ni-3Mn alloy and Al-4Ni-4Mn alloy presented 12% and 14% yield strength loss, respectively. Similarly, the ultimate tensile strength of the Al-4Ni alloy showed a 60% reduction while the Al-4Ni-2Mn alloy only showed 41%. The Al-4Ni-3Mn alloy and Al-4Ni-4Mn alloy presented 37% and 34% ultimate tensile strength loss respectively between 25°C and 250°C, being less than for the Al-4Ni alloy. It can thus be concluded that Mn addition can effectively improve the softening resistance of Al-4Ni alloys at evaluated temperatures.

Isothermal Holding at 250°C

To study the thermal stability of Al-Ni-Mn alloys, the Al-4Ni-2Mn alloy was held at 250°C for different times from 100 h to 2000 h. The microstructures are displayed in Fig. 4. The eutectic $Al_9(Ni,Mn)_2$ phase remained rod-like shape after 2000 h at 250°C, and no coarsening was observed. Moreover, no precipitates were observed in the primary α-Al after 2000 h at 250°C.

Table I. Volume fraction of different phases in experimental Al-Ni-Mn alloys

	Volume fraction (vol.%)		
Alloy	**Primary α-Al (%)**	**Eutectic phases (%)**	**Intermetallic phases (%)**
Al-4Ni	56	44	–
Al-4Ni-2Mn	49	51	–
Al-4Ni-3Mn	41	58	1
Al-4Ni-4Mn	35	60	5

Table II. Strength loss of Al-4Ni and Al-4Ni-*x*Mn alloys at 250°C

	Strength loss	
Alloy	**Yield strength (%)**	**Ultimate tensile strength (%)**
Al-4Ni	27	60
Al-4Ni-2Mn	10	41
Al-4Ni-3Mn	12	37
Al-4Ni-4Mn	14	34

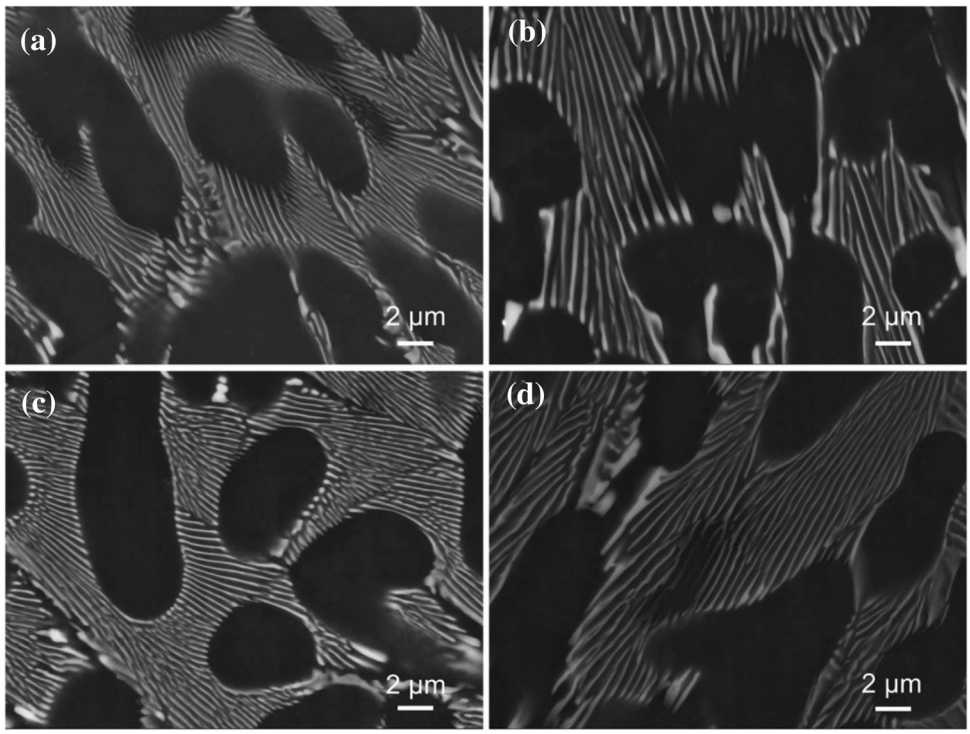

Fig. 4. Backscattered SEM micrographs showing microstructure of Al-4Ni-2Mn alloy after isothermal holding at 250°C for (a) 100 h, (b) 540 h, (c) 1000 h, and (d) 2000 h.

Figure 5 presents the Vickers hardness of the Al-4Ni-2Mn alloy after isothermal holding at 250°C for various times. The hardness showed no obvious change, and the fluctuation was within a very narrow range. The hardness increased from 64.5 HV_{10} for the as-cast sample to 69.0 HV_{10} after holding at 250°C for 540 h. The hardness after holding for 2000 h was still 68.1 HV_{10}.

The eutectic $Al_9(Ni,Mn)_2$ showed good stability at 250°C. However, the Al_3Ni phase is also thermally stable at 250°C. Hence, this is not sufficient to explain why the alloys with Mn addition experienced less strength loss. As mentioned above, the

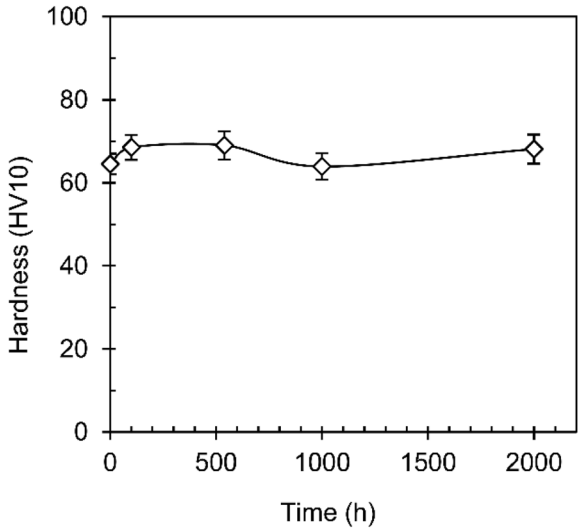

Fig. 5. Hardness of Al-4Ni-2Mn alloy after isothermal holding at 250°C for different times.

main difference between the Al-4Ni and Al-4Ni-2Mn alloys is the eutectic structure, which was Al_3Ni/α-Al and $Al_9(Ni,Mn)_2$/α-Al, respectively. Hence, the difference in their strength loss may be related to different softening behavior between $Al_9(Ni,Mn)_2$ and Al_3Ni phases. The microhardness of α-Al, Al_3Ni, and Al_9FeNi phases is reported in Ref. 30 No data for $Al_9(Ni,Mn)_2$ phase were reported, but Al_9FeNi phase was found. The Al_9FeNi[26] phase is also known as $Al_9(Fe,Ni)_2$; It shows the same monoclinic Al_9Co_2 structure as the $Al_9(Ni,Mn)_2$ phase. Also, the composition of Al_9FeNi phase was Al-13.4 at.%Ni-4.2 at.%Fe, close to that of the $Al_9(Ni,Mn)_2$ phase (Al-13.5 at.%Ni -3.7 at.%Mn). Moreover, Fe and Mn are next to each other in the Periodic Table. These two elements have very similar atomic radii (r_{Mn} = 1.40 Å, r_{Fe} = 1.26 Å) and can replace each other in many intermetallic phases. In addition, the Al_9FeNi phase and $Al_9(Ni,Mn)_2$ contain a relatively low level of Fe and Mn, respectively. It is thus expected that Mn atoms will replace Fe atoms. The Al_9FeNi and $Al_9(Ni,Mn)_2$ phase should present similar hardness and softening behavior at elevated temperatures.

The microhardness at different temperatures is shown in Fig. 6a. The microhardness of Al_9FeNi phase was 7.71 GPa at ambient temperature, while that of Al_3Ni was only 5.95 GPa. When the temperature was increased to 350°C, the hardness of the Al_9FeNi phase was 5.83 GPa while that of Al_3Ni was only 3.54 GPa. The Al_9FeNi phase showed higher hardness than the Al_3Ni phase at both ambient and elevated temperature. In addition, the hardness of the α-Al phase decreased dramatically from 1.45 GPa to 0.143 GPa when the temperature was increased to 350°C, indicating that the α-Al phase softens quickly at elevated temperatures. Figure 6b presents the fraction of the hardness remaining at elevated temperatures for the different phases. Clearly, Al_9FeNi phase retained higher hardness

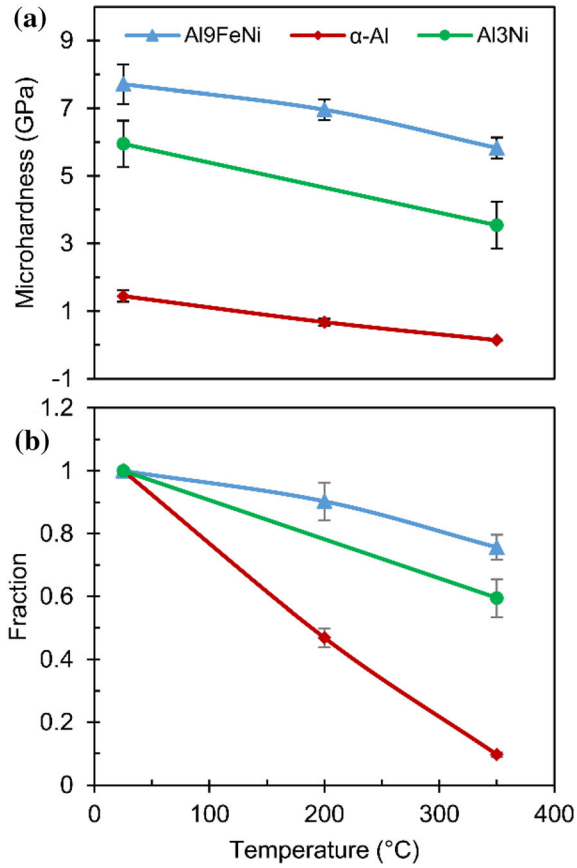

Fig. 6. (a) Microhardness of α-Al, Al_3Ni, and Al_9FeNi phases and (b) fraction of microhardness remaining at different temperatures.

than the Al_3Ni phase. When the temperature was increased to 350°C, the Al_9FeNi phase maintained 75.6% of its hardness while the Al_3Ni phase maintained only 59.5%. Hence, the Al_9FeNi phase showed better softening resistance than the Al_3Ni phase at elevated temperatures. Therefore, it is expected that the $Al_9(Ni,Mn)_2$ phase will also present higher softening resistance than the Al_3Ni phase. Similarly, the eutectic $Al_9(Ni,Mn)_2$/α-Al structure displayed better softening resistance than the Al_3Ni/α-Al structure. Therefore, the transformation of the eutectic from Al_3Ni to $Al_9(Ni,Mn)_2$ can improve the softening resistance with less strength loss at 250°C.

CONCLUSION

1. Mn addition transformed the eutectic intermetallic phase from Al_3Ni to $Al_9(Ni,Mn)_2$ phase. The $Al_9(Ni,Mn)_2$ phase showed rod-like shape. With increasing Mn content, k-phase, O-phase, and Al_6Mn phase formed as primary phases in Al-Ni-Mn alloys.
2. Mn addition significantly improved the mechanical performance of cast Al-4Ni alloy at ambient temperature and at 250°C. This improvement is due to the solid solution of Mn in α-Al and the

increase of eutectic phases and primary intermetallic phases with increasing Mn content.
3. Mn addition improved the softening resistance. Alloys with Mn addition presented less strength loss than the Al-4Ni alloy when the temperature was increased to 250°C. The eutectic $Al_9(Ni,Mn)_2$ phase displayed higher softening resistance than the Al_3Ni phase.
4. The eutectic intermetallic $Al_9(Ni,Mn)_2$ phase showed good thermal stability at 250°C. No coarsening was observed after 2000 h, and no precipitates were observed in α-Al. The hardness showed no decrease after isothermal holding at 250°C for up to 2000 h.

ACKNOWLEDGEMENT

Financial support from Jaguar Land Rover for Jiao Fang's PhD study is gratefully acknowledged.

CONFLICT OF INTEREST

On behalf of all authors, the corresponding author states that there is no conflict of interest.

OPEN ACCESS

REFERENCES

1. H. Ye, *J. Mater. Eng. Perform.* 12, 288. (2003).
2. K.E. Knipling, D.C. Dunand, and D.N. Seidman, *Z. Met.* 97, 246. (2006).
3. O. Elsebaie, A.M.A. Mohamed, A.M. Samuel, F.H. Samuel, and A.M.A. Ahmari, *Mater. Des.* 32, 3205. (2011).
4. W. Kasprzak, B.S. Amirkhiz, and M. Niewczas, *J. Alloys Compd.* 595, 67. (2014).
5. T. Gao, X. Zhu, Q. Sun, and X. Liu, *J. Alloys Compd.* 567, 82. (2013).
6. X.G. Chen, and M. Fortier, *J. Mater. Process. Technol.* 210, 1780. (2010).
7. Y. Li, Y. Yang, Y. Wu, L. Wang, and X. Liu, *Mater. Sci. Eng. A* 527, 7132. (2010).
8. J. Røyset, and N. Ryum, *Int. Mater. Rev.* 50, 19. (2005).
9. C.B. Fuller, D.N. Seidman, and D.C. Dunand, *Acta Mater.* 51, 4803. (2003).
10. M. Rahimian, S. Amirkhanlou, P. Blake, and S. Ji, *Mater. Sci. Eng. A* 721, 328. (2018).
11. Y. Harada, and D.C. Dunand, *Intermetallics* 17, 17. (2009).
12. H.A. Elhadari, H.A. Patel, D.L. Chen, and W. Kasprzak, *Mater. Sci. Eng. A* 528, 8128. (2011).
13. G. Liu, P. Blake, and S. Ji, *J. Alloys Compd.* 809, 151795. (2019).
14. R.E. Franck, and J.A. Hawk, *Scr. Metall.* 23, 113. (1989).
15. P.Y. Li, H.J. Yu, S.C. Chai, and Y.R. Li, *Scr. Mater.* 49, 819. (2003).
16. W.J. Golumbfskie, M.F. Amateau, T.J. Eden, J.G. Wang, and Z.K. Liu, *Acta Mater.* 51, 5199. (2003).
17. P.Y. Li, S.L. Dai, C.Y. Li, and B.C. Liu, *Acta Metall. Sin.* 12, 452. (1999).
18. V.S. Zolotorevsky, N.A. Belov, and M.V. Glazoff, *Casting Aluminum Alloys* (Elsevier, Amsterdam, 2007), pp 230–232.
19. V. Raghavan, *J. Phase Equilibria Diffus.* 27, 493. (2006).
20. Y. Fan, K. Huang, and M.M. Makhlouf, *Metall. Mater. Trans. A Phys. Metall. Mater. Sci.* 46, 5830. (2015).
21. H. Okamoto, *J. Phase Equilibria Diffus.* 25, 394. (2004).
22. J.L. Murray, and A.J. McAlister, *Bull. Alloy Phase Diagr.* 5, 74. (1984).
23. Å. Jansson, *Metall. Trans. A* 23, 2953. (1992).
24. S. Balanetskyy, G. Meisterernst, B. Grushko, and M. Feuerbacher, *J. Alloys Compd.* 509, 3795. (2011).
25. W. Yu, Q. Hao, L. Fan, and J. Li, *J. Alloys Compd.* 688, 798. (2016).
26. I. Chumak, K.W. Richter, and H. Ipser, *Intermetallics* 15, 1416. (2007).
27. A. Sato, A. Yamamoto, X.Z. Li, K. Hiraga, T. Haibach, and W. Steurer, *Acta Crystallogr. Sect. C Cryst. Struct. Commun.* 53, 1531. (1997).
28. G.V. Raynor, *J. Inst. Met.* 70, 507. (1944).
29. K. Robinson, *Acta Crystallogr.* 7, 494. (1954).
30. C.L. Chen, G.D. West, and R.C. Thomson, *Mater. Sci. Forum* 519–521, 359. (2006).